Experimental and Numerical Study on Detonation Propagating in an Annular Cylinder

Xudong Zhang, Baochun Fan*, Zhenhua Pan, Mingyue Gui, Zhihua Chen
Science and Technology on Transient Physics Laboratory, Nanjing University of Science and Technology,
Nanjing, Jiangsu 210094, China

1 Introduction

Various schemes have been proposed to control detonations in detonation-based engines, among which the rotating detonation engine (RDE) may be more suitable for space launch application due to many advantages compared to other concepts of detonation propulsions. In RDE, it has been confirmed by experiments[1-4] that a steadily rotating detonation can be established in an annular combustion chamber, which implies the distributions of the detonation strength along the detonation front are of ununiform. The fundamental question then arises on how the rotating detonation can be self-sustained.

In Ref [5], the experiments were conducted on the detonation propagating in a locally curved channel and a pipe with a bend, both expansion and compression effects of locally curved walls on the cellular structure were concerned, which can lead the detonation to propagate or to fail. The numerical studies were also carried out to identify the effects of curvature on the rotating detonation[6], but only the compression effect by the curved geometry was considered, which causes the detonation to be overdriven. However, these previous works can not reveal the self-sustaining propagation mechanism of rotating planar detonations exactly. In this paper, the flow features of rotating detonations in the annular chamber are investigated experimentally and numerically, and the self-sustaining propagation mechanisms are examined.

2 Experimental setup

The experimental setup shown in Figure 1 consists of detonation tube, annular combustor and detonation vent. A steady detonation is created in the detonation tube with a rectangular cross-section of 30 mm×15 mm and length of 2085 mm. The annular combustor with same rectangular cross-section connected with the detonation tube as a test section has an inner radius of 85 mm and an outer radius of 115 mm, The detonation vent used to prevent the distortion of the cellular record from the environment is connected with the exit of the test section and sealed with a thin paper on the open end.

Eight pressure gauges (P1-P8), grouped into four pairs, are mounted flush with the inside wall of the chamber as shown in Figure 1(a). One pair of gauges (P1-P2) are placed on the detonation tube, near the entrance of the annular chamber to monitor the C-J detonation and the rest of gauges are placed on the upper, outer and inner walls near the exit of the text section respectively, to monitor the rotating detonation in the chamber. The peak pressure and the propagating velocity of the detonation

Correspondence to: Baochun Fan. Email: bcfan@mail.njust.edu.cn.

thus can be measured and compared to that of a C-J detonation measured near the chamber entrance. In addition, the smoked foils are also mounted on the bottom of the annular chamber to record cellular patterns.

A stoichiometric hydrogen/oxygen mixture diluted with argon ($H_2/O_2/Ar = 2:1:3$) at an initial pressure of 85KPa and 280K is used as a combustible gas in experiments.

(a) Photograph of experimental setup

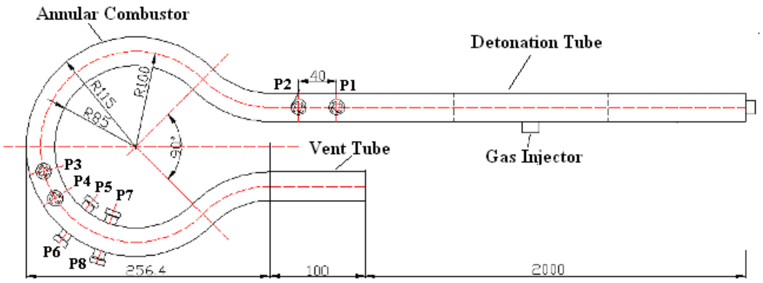

(b) Schematic of experimental setup

Figure 1. Experimental setup

3 Physical and numerical model

3.1. Governing equation and numerical method

The two-dimensional chemical non-equilibrium Euler equations in non-dimensional and generalized body-fitted (ξ,η) coordinates are given as

$$\frac{\partial \boldsymbol{Q}}{\partial t}+\frac{\partial \boldsymbol{F}}{\partial \xi}+\frac{\partial \boldsymbol{G}}{\partial \eta}=\boldsymbol{S}\,, \tag{1}$$

where,

$$\boldsymbol{Q}=\{\rho_1,\rho_2,\cdots,\rho_{Ns},\rho u,\rho v,E\}^T,$$

$$\boldsymbol{F}=\{\rho_1\overline{U},\rho_2\overline{U},\cdots,\rho_{Ns}\overline{U},\rho u\overline{U}+p\xi_x,\rho v\overline{U}+p\xi_y,\overline{U}(p+E)\}^T,$$

$$\boldsymbol{G}=\{\rho_1\overline{V},\rho_2\overline{V},\cdots,\rho_{Ns}\overline{V},\rho u\overline{V}+p\eta_x,\rho v\overline{V}+p\eta_y,\overline{V}(p+E)\}^T,$$

$$\boldsymbol{S}=\{\dot{\omega}_1,\dot{\omega}_2,\cdots,\dot{\omega}_{Ns},0,0,0\}^T,$$

$$\overline{U}=u\xi_x+v\xi_y\,,\ \overline{V}=u\eta_x+v\eta_y\,.$$

Here u and v are the velocity components in the physical (x, y) coordinates, ρ is the density of the mixture, $\rho=\sum_{k=1}^{Ns}\rho_k$, $\rho_k=\rho Y_k$, Y_k is the mass fraction of the k-th species; p is the pressure; E is the total energy per unit volume, $E=\rho\sum_{k=1}^{Ns}Y_k e_k+\rho\left(u^2+v^2\right)/2$, where e_k is the internal energy of the k-th species per unit mass. $\dot{\omega}_k$ is the mass production rate of k-th species, which is expressed as

$$\dot{\omega}_k=W_k\sum_{i=1}^{Nr}(\nu_{ki}^{''}-\nu_{ki}^{'})(k_{fi}\prod_{k=1}^{Ns}n_k^{\nu_{ki}^{'}}-k_{bi}\prod_{k=1}^{Ns}n_k^{\nu_{ki}^{''}}) \tag{2}$$

3.2. Computational model

The spatial derivatives of fluxes F, G in Equation(1) are integrated by the fifth-order weighted essentially non-oscillatory (WENO) scheme[7], where three candidate stencils are used and when the function has a discontinuity in a stencil, the corresponding weigh ω_r should be essentially 0, to eliminate the spurious oscillation near the discontinuity in calculations. The second-order additive semi-implicit Runge-Kutta Method[8] is employed to discretize the time term and tread the stiffness of the chemical source terms.

The computational domain is shown in Figure 2. The left and right sides are connected by the periodic boundary conditions. The inner and outer walls are considered as slip, adiabatic solid conditions defined as

$$\left.\frac{\partial\left(\bar{U}/\xi\right)}{\partial\xi}\right|_w = 0\,,\ \bar{V}\big|_w = 0\,, \tag{3}$$

which is wall curvature dependent. The grid number of the combustor is $\xi\times\eta$=120×800.

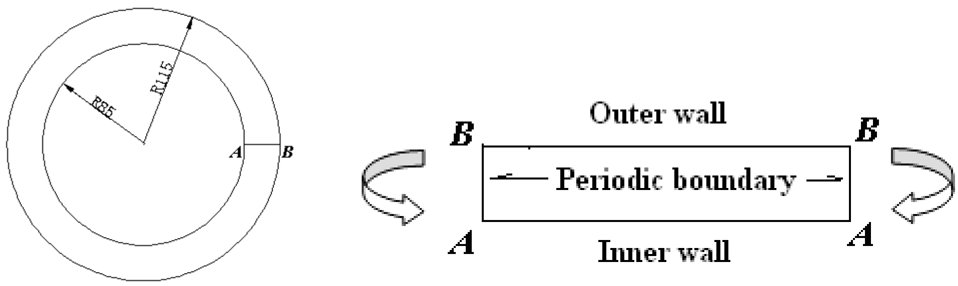

(a) physical domain (b) computational domain

Figure 2. Schematic diagram of computational domain

A detailed chemical reaction mechanism with 8 species and 48 elementary reactions[9] is employed and thermodynamic data of species can be found from the JANAF table[10].

4 Results and discussion

Typical pressure signals recorded by P6-P8 are shown in Figure 3, from which the pressure peaks and the propagation behaviors of the detonation can be detected. It has been found that the detonation rotates steadily with circular velocity $\omega = 1.68^{\circ}/s$ based on the measured velocities of the detonation D_{outer} =1728.5m/s , D_{middle} =1483.5m/s and D_{inner} =1252.5m/s , where D_{outer} , D_{middle} and D_{inner} are the detonation velocities measured by P6-P8, P3-P4 and P7-P9 respectively. In addition, the pressure on the outer wall of 2102kPa is higher then the pressure on the inner wall of 1693kPa.

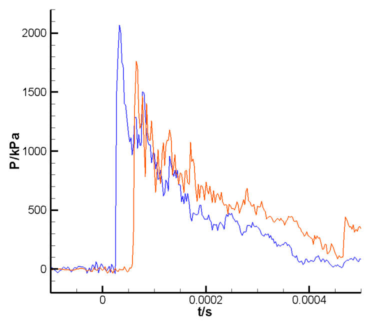

Figure 3. Pressure histories record by P6-P8

Figure 4(a) shows the measured cellular patterns of rotating detonations. It is observed that the cellular size near the outer concave wall is smaller considerably than that near the inner convex wall and the detonation front is continuously realigning itself to the local channel axis, to maintain the detonation steadily propagates with a planar front into the azimuthal direction.

It is well-known that the transverse wave emanating from the triple point in Mach configuration propagates laterally along the detonation front supports the main detonation wave and gives the cellular structure. The natural transverse spacing is related directly with the cell size and influenced by flowfields and strength of detonation. The wall effects existing in the annular combustor can change the flowfield and strength of detonation and thus change the cell size consequently. For example, near the outer wall, both the lesser extent pressure effect due to geometrical compression and the overdriven due to Mach reflection lead to the decrease of cell size as shown in Figure 4(a). The calculated cellular patterns shown in Figure 4(b) are in qualitative agreement with calculated results shown in Figure 4(a).

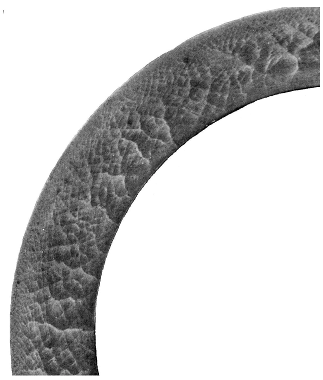

(a) Measured

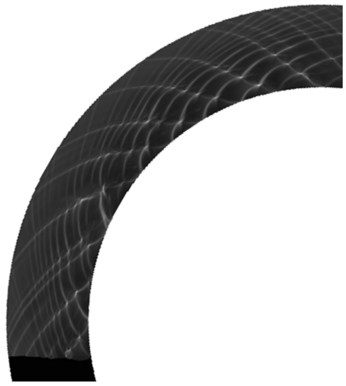

(b) Calculated

Figure 4. Smoke-foil records written by triple shocks in rotating detonation

Figure 5 is a calculated schlieren graph of pressure at a selected time, where the shock fronts and transverse waves are described sharply. It can be seen that the transverse spacing, which is related directly with the width of cell, decreases along radial direction and the fronts of transverse wave are inclined to the inner wall.

The shadow graph of H_2 mass fraction is shown in Figure 6, where the black line represents the leading shock front. The induction zone formed behind the relatively weak leading shock near the inner wall is larger than that near the outer wall, whereas the burning pockets penetrating into the burnt region can be detected, which depth decreases along radial direction. Therefore the reaction area near the inner convex wall is wider than that near the outer concave wall, and the strength of the outside detonation front is stronger than the inside portion

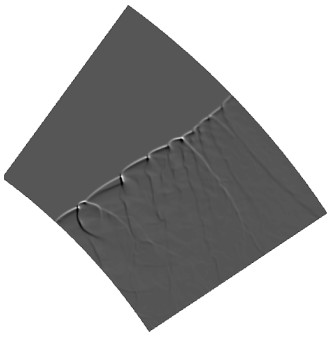

Figure 5. Calculated schlieren graph of pressure

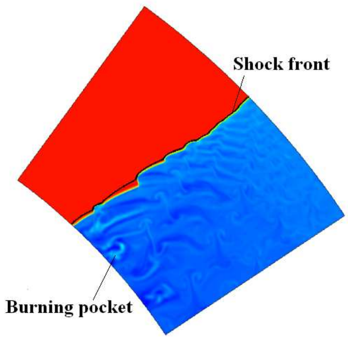

Figure 6. Shadow graph of H_2 mass fraction

5 Conclusions

Both the experimental and numerical studies on detonation propagating in an annular cylinder have been presented. The wall effects existing in the annular combustor influence the flowfield such as the transverse waves and strength of detonation, which leads to that the cellular size near the outer concave wall is smaller than that near the inner convex wall, the reaction area near the inner wall is wider than that near the outer wall, and the strength of the outside detonation front is stronger than the inside portion. Therefore the effects of the concave and convex walls permit a detonation to propagate with a constant circular velocity.

Acknowledgements

The work was supported by the natural science fund of China (No. 10872096)

References

[1] Voitsekhovskii BV. (1959). Stationary detonation. Doklady USSR Academy Sci. 129: 1254.

[2] Nicholls JA, Dabora EK, Gealler RA. (1959). Studies in connection with stabilized gaseous detonations waves. 11th Symposium on Combustion and Detonation: 766.

[3] Bykovskii FA, Vedernikov EF. (1996). Continuous detonation combustion of an annular gas-mixture layer. Combustion, Explosion and Shock Waves. 32: 489.

[4] Hishida M, Fujiwara T, Wolanski P. (2009). Fundamentals of rotating detonations. Shock Waves. 19: 1.

[5] Thomas GO, Williams RL. (2002). Detonation interaction with wedges and bends. Shock Waves. 11: 481.

[6] Lee SH, Jo DR, Choi JY. Effect of curvature on the detonation wave propagation characteristics in annular channels. AIAA 2008-988.

[7] Shu CW, Osher SJ. (1988). Efficient implementation of essentially non-oscillatory shock capturing schemes. J. Comput. Phys.. 77: 439.

[8] Oran ES, Young TR, Boris JP, et al. (1982). Weak and strong ignition. I. Numerical simulations of shock tube experiments. Combust Flame. 48: 135.

[9] Zhong XL. (1996). Additive semi-implicit Runge-Kutta methods for computing high-speed nonequilibrium reactive flows. J. Comput. Phys. 128: 19.

[10] Gordon S, McBride DJ. NASA Report SP-273, 1971.